**Climate
of the Past**

Open Access

Discussions

Coupled regional climate–ice sheet simulation shows limited Greenland ice loss during the Eemian

M. M. Helsen, W. J. van de Berg, R. S. W. van de Wal, M. R. van den Broeke, and J. Oerlemans

Institute for Marine and Atmospheric research Utrecht (IMAU), Utrecht University, Princetonplein 5, 3584 CC Utrecht, the Netherlands

Correspondence to: M. M. Helsen (m.m.helsen@uu.nl)

Discussion Paper | Discussion Paper | Discussion Paper | Discussion Paper |

CPD

9, 1735–1770, 2013

Limited Greenland ice loss during the Eemian

M. M. Helsen et al.

Title Page

Abstract	Introduction
Conclusions	References
Tables	Figures

|◀ | ▶|

◀ | ▶

Back | Close

Full Screen / Esc

Printer-friendly Version

Interactive Discussion

Full Screen / Esc

Printer-friendly Version

Interactive Discussion

Abstract

During the last interglacial (Eemian, 130–115 kyr BP) eustatic global sea level likely peaked at > 6 m above the present-day level, but estimates of the contribution of the Greenland ice sheet vary widely. Here we use an asynchronously two-way coupled regional climate–ice sheet model, which includes physically realistic feedbacks between the changing ice sheet topography and climate forcing. Our simulation results in a contribution from the Greenland ice sheet to the Eemian sea level highstand between 1.2 and 3.5 m, with a most likely value of 2.1 m. Simulated Eemian ice loss in Greenland is dominated by the rapid retreat of the southwestern margin: two-thirds of the ice loss occurred south of 70° N. The southern dome survived the Eemian and remained connected to the central dome. Large-scale ice sheet retreat is prevented in areas with high accumulation. Our results broadly agree with ice core inferred elevation changes and marine records, but it does not match with the ice-core derived temperature record from northern Greenland. During maximum Eemian summertime insolation, Greenland mass loss contributed ~ 0.5 m kyr^{-1} to sea level rise, 24 % of the reconstructed total rate of sea level rise. Next to that, a difference of > 3 m remains between our maximum estimate of the Greenland contribution and the reconstructed minimum value of the global eustatic Eemian highstand. Hence, the Antarctic ice sheet must also have contributed significantly to this sea level highstand.

1 Introduction

Eemian Arctic summer temperatures were 4–5 K higher than preindustrial values (CAPE-Last Interglacial Project Members, 2006; Overpeck et al., 2006), and reconstructions of peak eustatic global sea level rise (SLR) vary from 4 to 9 m above the present-day level (Jansen et al., 2007; Dutton and Lambeck, 2012; Kopp et al., 2009). The contribution of the Greenland ice sheet (GrIS) to the Eemian sea level highstand is uncertain. Interpretation of ice core records is controversial (Alley et al., 2010): some

studies suggest an almost complete deglaciation of southern Greenland and a substantially reduced central dome (Koerner, 1989; Koerner and Fisher, 2002); later studies claim the survival of the southern dome, based on the presence of Eemian ice at Dye-3 (NGRIP members, 2004). Moreover, the inclusion of biological material in the basal silty ice of the Dye-3 ice core dating back to > 400 kyr BP suggests that the ice sheet did not retreat from this location since then (Willerslev et al., 2007). Only minor ice thickness changes in central/northern Greenland are deduced from ice cores in this area (NGRIP members, 2004), a conclusion that is supported by the recent interpretation of the NEEM ice core, pointing to a minimum elevation of only 130 ± 300 m below the present-day surface (NEEM community members, 2013).

Ice sheet modelling experiments result in a broad spectrum of Eemian ice loss estimates, ranging from a sea level equivalent of 0.4 to 5.5 m, with a tendency towards higher mass loss estimates (Cuffey and Marshall, 2000; Huybrechts, 2002; Tarasov and Peltier, 2003; Lhomme et al., 2005; Otto-Bliesner et al., 2006; Robinson et al., 2011; Fyke et al., 2011; Born and Nisancioglu, 2012; Quiquet et al., 2013). The outcome of modelling experiments depends strongly on the method chosen to calculate the surface mass balance (SMB), being the sum of snowfall, sublimation and meltwater run-off. Often, a single temperature chronology is used derived from ice core records. This temperature is then used to estimate changes in accumulation and run-off, both based on lapse-rate considerations (Cuffey and Marshall, 2000; Tarasov and Peltier, 2003; Lhomme et al., 2005; Quiquet et al., 2013). This approach has the advantage of being computationally cheap, but strongly simplifies the complex nature of SMB changes. Alternatively, forcing fields from climate models can be used, such as for example has been done for the Eemian with time-slice (one-way) coupled climate–ice sheet model experiments, using a positive degree day approach to calculate melt (Otto-Bliesner et al., 2006; Born and Nisancioglu, 2012).

A physically more realistic approach to estimate the SMB is to use a regional climate model coupled to a multi-layer snow and ice melt model with prognostic albedo calculation. These models simulate modern GrIS SMB very well (Fettweis et al., 2008;

Limited Greenland ice loss during the Eemian

M. M. Helsen et al.

Title Page

Abstract | Introduction

Conclusions | References

Tables | Figures

◄◄ | ►►

◄ | ►

Back | Close

Full Screen / Esc

Printer-friendly Version

Interactive Discussion

Ettema et al., 2009), and can be considered a major improvement over coarse-gridded GCMs. This approach has also been successfully applied for past climate states (Van de Berg et al., 2011), using a fixed ice sheet topography. Here we two-way couple the regional atmospheric climate model RACMO2 (Van de Berg et al., 2011) to the thermomechanical ice sheet model ANICE (Helsen et al., 2012), using the extensively validated GCM ECHO-G as lateral forcing (Kaspar et al., 2005) (Sect. 2), to conduct a 15 kyr transient ice sheet–climate simulation of the GrIS over the Eemian interglacial. With this approach we do not only take advantage of the improved performance of regional climate models over GCMs (Otto-Bliesner et al., 2006), but moreover the two-way coupling ensures a physically realistic representation of the feedbacks between the continuously changing ice sheet topography and the climate forcing, and hence yields more confidence in the SMB reconstruction.

2 Methods

2.1 Coupled model set-up

The computational costs of high resolution (~ 20 km) atmospheric climate models limit maximum simulation periods to decades. Since we simulate the GrIS evolution over 15 kyr, one-to-one coupling of an ice sheet model and a climate model is not feasible at present for this type of study. As a viable alternative, we use an a-synchronous two-way coupling strategy, involving the 3-D thermomechanical ice sheet model ANICE (e.g. Van de Wal, 1999; Bintanja and Van de Wal, 2008; Helsen et al., 2012) and the regional atmospheric climate model RACMO2 (e.g. Ettema et al., 2009; Van de Berg et al., 2011). Every 1.5 kyr, fields of surface topography and ice mask are fed from the ice sheet model to the regional climate model. We compute a new climatology using appropriate boundary conditions (see below) and subsequently transfer modelled SMB, surface temperature and amount of refrozen meltwater to the ice sheet model. The latter is then run for another 1.5 kyr, etc. (Fig. 1). Changes are only applied to the

ice cover in Greenland, the ice in the Canadian Archipelago is left unchanged in the regional climate model. This coupling was performed 10 times, allowing an ice sheet-climate reconstruction from 130–115 kyr BP.

During ice sheet model simulations (in between model couplings), we continuously correct for the SMB-elevation feedback, using the SMB gradient method (Helsen et al., 2012). We recalculate the coefficients of SMB gradients for each Eemian climatology, using all RACMO2 grid points within a minimum search radius of 150 km. This radius is enlarged until a minimum number of H_s–SMB pairs ($n = 37$) is found, following Helsen et al. (2012).

Our modelling strategy involves multiple transfers of data products from the regional climate model to the ice sheet model and vice versa. As RACMO2 is run on a geographical based coordinate system, and ANICE on a (different) rectangular x-y grid, back and forth mapping and interpolating is inevitable; this is carried out using OBLIMAP, a coupler involving oblique stereographic mapping and a centre of projection at $40°$ W, $72°$ N (Reerink et al., 2010).

2.2 The regional atmospheric climate model

The Regional Atmospheric Climate Model version 2.1 (RACMO2) of the Royal Netherlands Meteorological Institute (KNMI) and adjusted at UU/IMAU for use over ice sheets, is used to calculate all Eemian climatologies used in this study (Ettema et al., 2009; Van de Berg et al., 2011). RACMO2 is run on a 18 × 18 km grid, with a domain size of 206 × 264 grid points (Fig. 1). It is forced at its boundaries by 6-hourly prognostic fields of temperature, humidity, wind, surface pressure, sea surface temperature and sea ice fraction from the ECHO-G global climate model (Kaspar et al., 2005, 2007). A detailed description of this set-up is given in Van de Berg et al. (2011). The performance of ECHO-G for the Eemian climate has been extensively validated with proxy records (Kaspar et al., 2005). The interior of the RAMCO2/GR domain is allowed to evolve freely. Each Eemian time slice climatology is based on the last 25 yr of a 30 yr simulation, to avoid spin-up effects.

Solar incoming radiation is adjusted for each Eemian time slice simulation to account for the influence of orbital forcing (Fig. 2, Berger and Loutre, 1991). For each Eemian time slice experiment, the ECHO-G forcing fields are adjusted to account for a changing ambient climate during the simulated period. The changing boundary conditions are based on two ECHO-G climatologies: Eemian Optimum (EO) and Glacial Inception (GI) (Kaspar et al., 2007). We used an interpolated climatology as forcing for RACMO2. Differences in monthly means between GI and EO are calculated for each forcing field (X). Subsequently, a fraction (f) of these differences is added to the EO fields for each time slice experiment, to account for the changing boundary conditions through the Eemian:

$$X_t = X_{EO} + f\left(\overline{X}_{GI} - \overline{X}_{EO}\right). \tag{1}$$

The value of f is set proportional to JJA insolation at 60° N, with $f = 1$ at 115 kyr BP and $f = 0$ at 125 kyr BP (Fig. 2). This approach allows a gradual transition of the climate forcing from the Eemian optimum to glacial inception. We used $f = 0$ for time slices between 130 and 125 kyr BP (hence maximum ambient air temperature), since we only wish to use the scaling procedure for interpolation between the two climatologies, not for extrapolation. This is justified by paleoclimatic evidence for already high global temperatures (Winograd et al., 1997; CAPE-Last Interglacial Project Members, 2006; EPICA community members, 2006) and greenhouse gases (Petit et al., 1999; Siegenthaler et al., 2005) during this time.

2.3 The ice sheet model

We use the 3-D thermomechanical model ANICE (Van de Wal, 1999; Bintanja and Van de Wal, 2008; Graversen et al., 2011; Helsen et al., 2012) based on the shallow ice approximation (SIA, Hutter, 1983), and explicitly accounting for the temperature-dependent stiffness of the ice. Ice temperature is calculated based on the 3-D advection, diffusion, friction, geothermal heat flux (G) at the bottom and annual surface

Full Screen / Esc

Printer-friendly Version

Interactive Discussion

temperature (T_s) adjusted for the effect of refreezing (Helsen et al., 2012). The vertical dimension is scaled with the local ice thickness, and consists of 15 layers with increasing resolution near the bed, to better resolve the local large gradient in ice velocity. For areas where basal temperatures reach the pressure melting point we allow the ice to slide over its bed, by using a Weertman-type sliding law (Weertman, 1964), corrected for the effect of subglacial water pressure (Bindschadler, 1983). Formation of ice shelves is not allowed; as soon as the ice starts to float, it breaks off. As such, calving by means of a floatation criterion is included, but calving physics are not explicitly incorporated, since model resolution and dynamics are not suited for a more realistic treatment of marine terminating outlet glaciers. The response of a changing ice load on bedrock elevation is taken into account using an Elastic Lithosphere–Relaxing Astenosphere (ELRA) model (Le Meur and Huybrechts, 1996). The different model components (ice flow, thermodynamics, SMB forcing and bedrock response) are applied on a rectangular domain of 141 × 77 grid points with a grid spacing of 20 km. Table 1 summarises the ice sheet model parameter values.

ANICE describes sheet flow (SIA), which is the dominant flow type over the major part of the GrIS. Although it is known that fast-flowing outlet glacier dynamics are not well-captured by this approximation, we argue that the errors introduced by the omission of this type of flow are minor, since the ice sheet quickly retreated on land during the Eemian, strongly reducing the influence of marine-terminating outlet glaciers dynamics.

Although Ellesmere Island is partly within the domain of the ice sheet model, and hence ice sheet changes in this region are also simulated, we do not include these in the computation of our ice volume changes.

3   Initialisation

The size and shape of the GrIS at the start of the Eemian are important, but poorly constrained initial conditions for this simulation. The response of the ice sheet to Eemian

Limited Greenland ice loss during the Eemian

M. M. Helsen et al.

warming will partly depend on the temperature history before the Eemian, due to the temperature-dependence of the ice viscosity (Fig. 3). For a realistic simulation of the GrIS response to Eemian warming, the influence of the preceding glacial cycle on size, shape and ice temperatures should therefore be taken into account. To this end, we

5 performed an experiment that simulates GrIS evolution through the penultimate glacial cycle, from ~ 237 to $\sim 130\,\mathrm{kyr\,BP}$.

Ice core records from Greenland do not cover the penultimate glacial cycle, so we need to rely on an ice core-derived climate record from Antarctica. Figure 4a shows that temperature histories for Greenland (GRIP, Johnsen et al., 2001) and Antarctica

10 (Vostok, Petit et al., 1999) differ considerably. We show the Vostok record for the period before 105 kyr BP, since the GRIP record is disturbed due to ice-flow irregularities prior to this date (NGRIP members, 2004). Most notable differences are a much smaller temperature amplitude and less high-frequency variability in the Vostok record. Therefore, both records are converted to a glacial index GI_t (Fig. 4b), such that GI = 1 represents

15 Last Glacial Maximum (LGM) conditions and GI = 0 corresponds to present-day conditions, following Greve (2005). The black line represents the GI_t signal after applying a Gaussian filter with a 2 kyr filter width. The red line shows the original variability in the GRIP record, which is much higher. The inset in Fig. 4b shows a scatter plot of the standard deviation in GI over a 3 kyr moving average as a function of the mean

20 GI, and illustrates that glacial conditions are characterised by larger variability than during Holocene conditions. It is likely that the penultimate glacial cycle in Greenland was also characterised by such high-frequency variability. Using the linear regression in this scatter plot (blue line: $\sigma_{\mathrm{GI}} = 0.05 + 0.24\,\mathrm{GI}$) and a random number generator we added high-frequency variability to the 3 kyr mean GI curve (Fig. 4c), which can then

25 be regarded as a potential temperature history over Greenland for the period prior to the Eemian.

This temperature history was used as forcing for the ice sheet model prior to 130 kyr BP. We use the SMB gradient method (Helsen et al., 2012) to calculate a direct adjustment of the SMB as a function of temperature perturbations. The present-day

SMB field (Ettema et al., 2009) is used as input for this method, and spatial SMB gradients within this field are calculated. Following Helsen et al. (2012), the temperature forcing as derived above is translated into a climatic elevation change ($\Delta H_{\text{climate}}$) using an atmospheric lapse rate $\gamma_{\text{atm}} = -7.4\,\text{K}\,\text{km}^{-1}$. Due to the spatially variable SMB gradients, a single temperature perturbation is translated into a spatially distributed SMB adjustment.

The resulting simulated ice volume over the last 2 glacial cycles is shown in Fig. 4d. Maximum ice volume ($3.70 \times 10^{15}\,\text{m}^3$) occurs at 136 kyr BP, following growth during the penultimate ice age. Ice sheet retreat occurs during the glacial termination, as well as interior thickening as a consequence of increased accumulation. For example, surface elevation at NEEM increased with 140 m between 135 and 130 kyr BP (not shown). We start our coupled regional climate–ice sheet model experiments at 130 kyr BP, with an ice sheet volume of $3.60 \times 10^{15}\,\text{m}^3$ (indicated by the red cross in Fig. 4d), 24 % larger than today. This is also the state of the ice sheet at the start of the Supplementary Movie.

4 Results

4.1 Eemian GrIS changes

The immediate response to the warm Eemian forcing (Fig. 2) is a decrease in ice volume (Fig. 5). The calving flux remains significant as long as large parts of the ice sheet are marine-terminating, but quickly diminishes when the ice sheet retreats on land. From then on, the ice loss is dominated by a decreasing SMB, mainly driven by increased summertime meltwater runoff. The dashed lines in Fig. 5a represent the ice sheet evolution when simulations are continued without additional coupling with the regional climate model. Acceleration of the mass loss occurs after each coupling interval until the insolation maximum at 125 kyr BP (Figs. 2 and 5). Ablation rates along the southwestern margin (Fig. 6) are enhanced by the growing area of dark tundra

Title Page

Abstract   Introduction

Conclusions   References

Tables   Figures

◄   ►

◄   ►

Back   Close

Full Screen / Esc

Printer-friendly Version

Interactive Discussion

that is exposed when the ice sheet retreats. Maximum local ablation values reach $3500\,\mathrm{kg\,m^{-2}\,yr^{-1}}$.

A persistent feature throughout the Eemian is the local SMB maximum at 50° W, 72° N (Fig. 6a). This is caused by high bedrock elevation, forming a promontory in the ice sheet, enhancing snowfall. As such, it acts as a topographic pinning-point for the ice sheet, as wet areas react less sensitively to warming than dry areas: frequent snowfall events keep the surface albedo high, and more melt is needed before the winter snow is removed in the ablation season, thus delaying exposure and melt of the darker ice. This locally prevents a retreat of the ice sheet and as a result this promontory demarcates the northern limit of rapid ice sheet retreat.

Another consequence of topographically forced precipitation in the west is the early readvance of the southwestern margin at 122.5 kyr BP, when the ice sheet still retreats along the dry northern margin (Supplement). GrIS volume increase starts again at 121 kyr BP, following decreasing summertime insolation and Northern Hemisphere cooling (Fig. 2).

Although retreat of the northern margin occurs, ice loss in this area is limited in comparison to other recent model studies of Eemian GrIS evolution (Robinson et al., 2011; Fyke et al., 2011; Born and Nisancioglu, 2012). A strong retreat of the northern margin does not agree with available ice core evidence (see Sect. 5). According to our results, 64 % of the total volume loss occurred south of 70° N, by strong retreat from the southwestern ice margin (Fig. 6c). Nevertheless, the southern dome survived, and remained connected to the central dome, due to persistent high accumulation (SMB > 0) along the southeastern ice margin, comparable to the present-day pattern. As a result, the remaining ice volume in south Greenland is substantially larger than in several other studies (Cuffey and Marshall, 2000; Huybrechts, 2002; Tarasov and Peltier, 2003; Lhomme et al., 2005; Otto-Bliesner et al., 2006).

The (near-)absence of ice in southern Greenland in previous studies is likely caused by underestimated accumulation in the southeast. Recent studies using climate forcing fields with high precipitation in this area result in continuous ice cover in southeast

Greenland (Fyke et al., 2011; Born and Nisancioglu, 2012; Quiquet et al., 2013). In our simulation, a band of high accumulation maintains significant ice discharge into the Irminger Sea. This mass flux remains relatively constant throughout the Eemian (blue dotted line in Fig. 5b), and accounts for most ($\sim 90\%$) of the calving during the period of minimum ice sheet extent. Except for this southeastern section, the ice sheet loses contact with the ocean in the first few kyr of ice sheet retreat, after which the magnitude and pattern of ice loss is mainly determined by the SMB. During this latter period, details of outlet glacier dynamics are likely to be of less importance. As a result, the uncertainty in SMB outweighs other sources of uncertainty, such as that in ice discharge by marine-terminating outlet glaciers (Sect. 4.3 and Fig. 7).

4.2 Ice sheet contribution to sea level

During the retreat phase (128–122 kyr BP), mass loss in the order of $\sim 180\,\mathrm{Gt\,yr^{-1}}$ ($\sim 0.5\,\mathrm{m\,SLR\,kyr^{-1}}$) is sustained for several millennia (Fig. 5b). Although surface lowering in the ablation zone increases the surface mass loss, this effect is counteracted by the fact that the lowest parts of the ablation area, where run-off rates are highest, disappear when the ice margin retreats. This limits the magnitude of the mass loss that can be sustained, similar to what happens to retreating valley glaciers.

These feedbacks between changing ice sheet extent and its climate forcing also explain the difference with an earlier study using the same regional climate model (Van de Berg et al., 2011), but assuming an unchanged present-day value of ice discharge and a fixed topography, resulting in a larger GrIS mass loss equivalent to $1.1\,\mathrm{m\,SLR\,kyr^{-1}}$. Eemian SMB attains a minimum value of $60 \pm 76\,\mathrm{Gt\,yr^{-1}}$ at 124 kyr BP in our simulation (Fig. 5b), which agrees closely to Van de Berg et al. (2011), although spatial differences exist due to the use of different ice sheet topography and extent. Hence it does not affect the outcome of our results.

The minimum ice sheet volume of $2.35 \times 10^{15}\,\mathrm{m^3}$ is reached at 121 kyr BP, and equals a $+2.1\,\mathrm{m}$ contribution to eustatic sea level. This value has been obtained by comparing simulated ice volume at 121 kyr BP to the simulated steady-state ice volume

for the present-day climate using the same regional climate–ice sheet modelling approach (Helsen et al., 2012). This means that a zero contribution to sea level rise is assumed for an ice volume of $3.2 \times 10^{15} \, \mathrm{m}^3$, which is 10 % larger than the observed present-day ice volume. This excess ice in both the simulated steady-state ice sheet (Helsen et al., 2012) and the Eemian ice sheet is predominantly found along the eastern margin (Fig. 6d), due to suboptimal representation of narrow outlet glacier dynamics. Since there is currently no ice in this area, we can safely assume that this excess ice was also absent during the minimum Eemian extent.

4.3 Sensitivity experiments

We explored the uncertainty of our results by performing eight sensitivity experiments (Table 2 and Fig. 7). These experiments could not be performed in the same coupled set-up as our control simulation, since this would require an additional ten 30 yr RACMO2 climate runs for each sensitivity experiment, which is computationally not feasible. We therefore conducted offline ice sheet model sensitivity experiments, using the ten control Eemian SMB climatologies, and calculated deviations of this SMB using the SMB gradient method (Helsen et al., 2012). This allows the ice topography to evolve freely throughout the simulated period, while SMB adjustments are made as a function of the difference with the surface elevation in the control run. Note that this method is also used in the control simulation, in between the couplings with the climate model.

4.3.1 Start of the warming

One of the uncertainties is the start of Eemian warm period, for which $130 \pm 1 \, \mathrm{kyr} \, \mathrm{BP}$ is a commonly used date (Jansen et al., 2007). Starting the simulations 1 kyr earlier/later obviously leads to an earlier/later onset of ice sheet retreat, but no additional non-linear effects are introduced, i.e. the rate of ice sheet retreat remains unaffected (Fig. 7a).

This effect results in a 0.3 m uncertainty in the contribution to sea level at the time of minimum ice sheet extent.

4.3.2 Sliding

A moderate uncertainty is introduced by the parameterisation of sliding over the bed. We doubled and halved the sliding velocity by adjusting the sliding coefficient, resulting in a −0.4 to +0.6 m SLR uncertainly (Table 2 and Fig. 7a). It should be noted that the sliding coefficient is usually used as a tuning parameter. Testing the full model sensitivity for a change in this parameter would require a new tuning and initialisation for each new parameter setting. This would considerably reduce the sensitivity of our results. The experiment conducted here represents a sudden increase/decrease of sliding velocity at 130 kyr BP, providing an upper estimate of the uncertainty in sliding behaviour.

4.3.3 Marine basal melt

An extra mass loss term is introduced by allowing melt at the marine interface of the ice sheet. We tested two values of this melt rate, based on realistic modern-day ice front retreat observations, i.e. 100 and 1000 m yr^{-1}. The ice sheet model uses a fixed grid, so we cannot directly apply these values to grounding line retreat. Alternatively, these retreat rates are assumed to operate on the vertical ice front that is in contact with the ocean. The equivalent mass loss occurring at the ice-ocean surface interface (in kg) is transferred to ice thinning of the grounded ice point bordering the ocean. This eventually results in ungrounding and thus calving in our model.

Obviously this mechanism only affects marine-terminating glaciers. As most of the ice sheet perimeter has retreated onto land at ∼ 128 kyr BP, the influence of marine basal melt ceases after the first 2 kyr of the simulation. The experiment with a marine basal melt of 100 m yr^{-1} did not significantly change the result of the control simulation.

Using 1000 m yr^{-1} melt rate at the ice–ocean interface resulted in an additional ice volume loss of 0.3 m SLR.

4.3.4 SMB

Constraining the uncertainty resulting from the SMB forcing in our study is not straight-forward. Van de Berg et al. (2011) report an uncertainty of 76 Gt yr^{-1} for their Eemian GrIS SMB reconstruction. We essentially use the same SMB product, although the SMB is based on a different ice sheet topography for each time slice. Since we calculate SMB adjustments based on a deviation between the simulated ice sheet elevation and the elevation (H_s) as used in the subsequent climate model simulations, we are able to introduce an additional SMB offset by shifting our H_s–SMB functions over a certain ΔH_s. Tests using the present-day ice sheet topography (as also used in Van de Berg et al., 2011), revealed that a 100 m shift of H_s results in a ΔSMB of 76 Gt yr^{-1}. The sensitivity runs for SMB (Fig. 7b) are obtained using this ±100 m offset in H_s. This SMB uncertainty (contributing an additional +1.2 m SLR in the minimum SMB scenario) dominates the total uncertainty estimate (Fig. 7b), indicating the the Eemian minimum is determined by the accuracy of the SMB calculations.

The 76 Gt yr^{-1} uncertainty in SMB represent the uncertainty in the model results for RACMO2. On top of that, there is an uncertainty from the choice of the GCM used as lateral forcing fields for RACMO2. Here we chose ECHO-G, but a choice for a different GCM would result in different results. This source of uncertainty is hard to quantify, since it would need a suite of experiments using different lateral forcing fields, which has not been performed for Eemian conditions yet. The Eemian climate run from ECHO-G is extensively validated against proxy data on temperature, which shows a ∼ 2 K warming in Europe (Kaspar et al., 2005). This is also in line with an independent reconstruction based on pollen data found in marine sediments in the Bay of Biscay (Sánchez Goñi et al., 2012). We can further compare simulated July temperatures in Baffin Island with proxy records, as this is an area within the RACMO2 domain. We

find 3 to 4 K higher July temperatures here, which is close to, but slightly lower than, the 4 to 5 K higher summertime temperatures as reconstructed from a compilation of paleoclimatic evidence (CAPE-Last Interglacial Project Members, 2006). A reconstruction of lake water temperatures on Baffin Island even found 5 to 10 K higher summer temperatures (Francis et al., 2006), but stronger than average warming of lake water can be explained by direct heating of the lake water due to the higher Eemian summertime insolation. Overall, the comparison with the available paleoclimatic evidence yields confidence in the quality of the Eemian climate from ECHO-G.

4.3.5 Total uncertainty

We realise that the total model uncertainty might be larger than captured by the above-mentioned components. However, paleoclimatic evidence from ice and marine cores can also be used to constrain the total uncertainty of our results (see Sect. 5). This comparison refutes a larger retreat of the southern part of the GrIS than the minimum SMB scenario, while larger retreat of the northern part of the GrIS is not in line with ice cores in this area (see Sect. 5). We therefore argue that the uncertainty in the SMB, and henceforth in the total GrIS contribution to SLR is adequately estimated.

The uncertainty estimates in the different time series in Figs. 5, 7 and 8 reflect the RMS difference between the individual sensitivity experiments and the control run, assuming that the different contributions are independent. Note that the uncertainty in total mass balance (black line in Fig. 5b) is very small. This is due to the strong dependency of calving on SMB: experiments with high (low) SMB result in larger (smaller) ice sheets that have more (less) contact with the ocean, and hence a larger (smaller) calving flux. Thus, total ice sheet mass balance features much less variability in the different experiments then its individual components SMB and calving flux.

5   Comparison to paleoclimate proxies

5.1   Marine records

Well-studied marine sediment sequences have been retrieved from a site close to southern Greenland in Eirik Drift. This site provides evidence for a reduced, but continuous presence of ice in southern Greenland during the Eemian (Carlson et al., 2008; Colville et al., 2011), which is in agreement with our model results. Next to that, De Vernal and Hillaire-Marcel (2008) use pollen records from this same site to provide evidence of an extensive increase in vegetation in southern Greenland. This also supports our reconstruction of the exposure of a large tundra area in southwest Greenland.

5.2   Ice core records

Figure 8 shows simulated Eemian surface height and temperature changes for five deep drilling locations, together with reconstructions from ice core interpretation. The NEEM ice core is the only record from Greenland that covers the complete Eemian (up to an age of 128.5 kyr BP), which is shown as the dark grey lines in Fig. 8. The other ice cores are assumed to contain Eemian ice, but no complete reconstruction of the Eemian climate can be retrieved due to disturbed chronologies (NGRIP members, 2004). Nevertheless, a consistent 3‰ higher isotopic composition in the (presumably) Eemian segments of the Camp Century, NGRIP, GRIP and GISP2 ice cores suggests only a minor drop (~ 100 m) in surface elevation of central and northern Greenland during the Eemian (NGRIP members, 2004). This lower limit of ice sheet thinning is depicted by the grey dashed lines in the left panels of Fig. 8. This value agrees with the NEEM reconstruction, that points to a minimum elevation in the Eemian of 130 ± 300 m below the present-day (NEEM community members, 2013).

The simulated elevation at NGRIP remained constant, while GRIP, NEEM and Camp Century experienced limited reductions in surface height (~ 140, 250, 300 m, respectively). If we compare these values with ice core reconstructions, the simulated change

in surface elevation compares well for NEEM, only the timing of the minimum is 1.3 kyr later in our simulation. Also at NGRIP our simulation remains within the maximum estimate of 100 m elevation decrease. Slightly larger thinning is found for Camp Century and GRIP, but remain within the uncertainty estimate for these locations. The larger (downward) uncertainty range demonstrates the sensitivity of surface elevation to mass loss rates in case of stronger warming scenarios (see below).

The deep drilling sites are currently located on the ice divide. However, this has likely not been the case during the entire Eemian: the ice divide moved southward at NEEM and Camp Century, whereas it moved northward from GRIP. NGRIP has been in the vicinity of the divide throughout the Eemian, resulting in a relatively stable surface elevation. The timing of the minimum surface elevation at the different locations is not synchronous, as a result of the out-of-phase response of the southwestern and northern parts of the GrIS.

For Dye-3 a maximum elevation drop during the Eemian of 500 m has been proposed (NGRIP members, 2004). Our results deviate significantly from this: in our reconstruction for Dye-3, ice free conditions start at 123 kyr BP, but the distance to the ice margin never exceeds 2 grid points (~ 57 km). Although Dye-3 is ice-free during ~ 5 kyr in most of the sensitivity experiments (Fig. 7), the most conservative experiment retains a continuous, shallow ice cover at Dye-3. Our results therefore do not exclude that localised ice cover persisted at Dye-3, which would explain the preservation of ancient (> 400 kyr BP) biological material in the basal ice (Willerslev et al., 2007). Otherwise, our results compare favourably with reconstructions of elevation changes based on ice cores from central and north Greenland (NGRIP members, 2004; NEEM community members, 2013), which suggest that Eemian ice thickness of the north and central ice sheet was close to its present value, whereas ice thickness in the south was substantially reduced.

A different picture emerges when we compare our results to ice core-derived temperature reconstructions (right panels of Fig. 8). NEEM community members (2013) deduce a maximum warming of 8 ± 4 K above the mean for the last millennium for NEEM,

Limited Greenland ice loss during the Eemian

M. M. Helsen et al.

whereas NGRIP members (2004) reconstructed a +5 K Eemian optimum temperature for central and northern Greenland. Our simulated temperatures remain well below these temperature reconstructions (Fig. 8). The ice core record concerns mean annual temperature, which implies that summertime warming must have been even larger, considering the increased summertime insolation in Greenland during the Eemian. This would induce even larger melt rates.

An important factor in the temperature reconstruction from NEEM community members (2013) is that corrections are made for elevation changes such that temperature on a constant elevation (the present-day surface) is reported. Especially in the early Eemian, ice-core derived elevation is above this value (and above our simulated elevation), which leads to higher reconstructed temperatures. Our simulated temperatures are actual surface temperatures, and hence affected by elevation changes. Temperature differences are still substantial between 125 and 117 kyr BP, but for this period our simulated temperatures overlap within the NEEM uncertainty estimate. In spite of these large differences in temperature, we do find extensive occurrence of surface melt at the NEEM location, in agreement with the ice core evidence (NEEM community members, 2013).

An Eemian warming of 8 K at NEEM would imply an additional 6 K warming at 124 kyr BP in our simulation. At that time, NEEM elevation is closest to the local equilibrium line altitude (ELA = 1582 m), though still 850 m higher. Taking $\gamma_{atm} = 7.4$ K km^{-1}, this implies that 6 K additional warming would bring the ELA to approximately the local elevation. Although our control simulation does not come close to these conditions, a short duration of such strong warming cannot be ruled out. Experiments with such warming (not shown) reveal that the additional mass loss downstream of NEEM would be very large, and the associated surface drawdown (~ 0.3 m yr^{-1}) would lead to ablation conditions at NEEM within two centuries. This in turn is in disagreement with ice core evidence, which suggests only minor surface height changes and continuous accumulation conditions throughout the Eemian.

Summarising, the comparison of elevation and temperature changes reveals a profound disagreement: if Greenland temperatures in our simulation would have been higher, this would improve the agreement with ice core-derived temperatures, but also induce significantly larger ice sheet retreat (and even conditions with negative SMB at NEEM), deteriorating the comparison with proxy elevation changes. It is difficult to reconcile the ice core interpretation of both a relatively stable ice sheet elevation in combination with a strong (5–8 K) Eemian warming over several millennia, certainly considering that summertime warming must have been even greater.

There are numerous complicating factors when a comparison is made between simulation results and proxy data: e.g. ice core-derived reconstructions of elevation and temperature rely on transfer functions involving assumptions on the relation between gas content and elevation, and the isotopic composition and temperature, respectively; a difference exists between elevation of the accumulation site and current ice core location; seasonality effects have to be taken into account. The presence of Eemian ice in ice cores from Camp Century, NEEM, NGRIP, GRIP and GISP2 that accumulated at altitudes similar to present-day, provides an important constraint on the estimate of total uncertainty estimate in our results: our minimum SMB scenario results in very strong surface lowering compared to the paleo evidence, which appears to preclude an even larger uncertainty in the downward (warm) direction.

5.3 Implications for sea level reconstructions

Our sensitivity experiments combined with the available geological evidence from ice (NGRIP members, 2004; Willerslev et al., 2007; NEEM community members, 2013) and marine cores (Carlson et al., 2008; De Vernal and Hillaire-Marcel, 2008; Colville et al., 2011) strongly suggest that the GrIS contribution to the Eemian sea level highstand was between 1.2 and 3.5 m, with a best estimate of 2.1 m (Fig. 5). Freshwater sources other than the GrIS are needed to explain the global sea level curve during the Eemian (Kopp et al., 2009); a difference of 3.1 m remains between our maximum estimate (3.5 m) of the GrIS contribution and the minimum SLR of 6.6 m (95 % probability)

(Kopp et al., 2009). The thermosteric plus mountain glacier and ice caps contribution probably did not exceed 1 m (Radić and Hock, 2011; McKay et al., 2011), implying that the Antarctic ice sheet must have contributed at least 2.1 m. If we adopt our minimum GrIS estimate (1.2 m) and the maximum estimated sea level highstand of 9.4 m (33 % probability) (Kopp et al., 2009), this leaves the possibility of an Antarctic contribution of 7.2 m, implying a contribution from both the West and East Antarctic Ice Sheets (Bamber et al., 2009; Pollard and DeConto, 2009).

The calculated rate of Greenland ice loss is only 9 % of the total rate of SLR of $\geq 5.6 \, \mathrm{m \, kyr^{-1}}$ at 127 kyr BP. This value (Kopp et al., 2009) includes a contribution from the Laurentide ice sheet, as it is reconstructed for global sea levels between 0 and -10 m. After 126 kyr BP the rate of SLR decreases to $\geq 2.1 \, \mathrm{m \, kyr^{-1}}$ (95 % probability) for sea levels ≥ 0 m (R. Kopp, personal communication, 2012); the GrIS contribution to this Eemian SLR totalled ≤ 24 %. Hence, also in terms of rate of change, our results require a significant Antarctic contribution to explain the estimates of the eustatic Eemian sea level curve.

6 Summary and conclusions

Based on a two-way coupled regional climate–ice sheet modelling approach, we conclude that GrIS retreat during the Eemian was dominated by SMB changes, and contributed 1.2–3.5 m to the maximum sea level highstand, with a best estimate of 2.1 m. This estimate broadly agrees with paleo ice sheet reconstructions from marine records (Carlson et al., 2008; De Vernal and Hillaire-Marcel, 2008; Colville et al., 2011) and ice cores (NGRIP members, 2004; Willerslev et al., 2007; NEEM community members, 2013), although an substantial disagreement with ice core-derived temperatures remains to be explained. The limited sea level contribution of the GrIS implies that a significant contribution of the Antarctic ice sheet is needed to explain the total Eemian sea level highstand.

References

Alley, R. B., Andrews, J. T., Brigham-Grette, J., Clarke, G. K. C., Cuffey, K. M., Fitzpatrick, J. J., Funder, S., Marshall, S. J., Miller, G. H., Mitrovica, J. X., Muhs, D. R., Otto-Bliesner, B. L., Polyak, L., and White, J. W. C.: History of the Greenland Ice Sheet: Paleoclimatic insights, Quaternary Sci. Rev., 29, 1674–1790, 2010. 1736

Bamber, J. L., Riva, R. E. M., Vermeersen, B. L. A., and LeBrocq, A. M.: Reassessment of the potential sea-level rise from a collapse of the West Antarctic ice sheet, Science, 324, 901–903, doi:10.1126/science.1169335, 2009. 1754

Berger, A. and Loutre, M. F.: Insolation values for the climate of the last 10 million years, Quaternary Sci. Rev., 10, 297–317, 1991. 1740

Bindschadler, R.: The importance of pressurized subglacial water in separation and sliding and the glacial bed, J. Glaciol., 29, 3–19, 1983. 1741

Bintanja, R. and Van de Wal, R. S. W.: North American ice-sheet dynamics and the onset of 100,000-year glacial cycles, Nature, 454, 869–872, 2008. 1738, 1740

Born, A. and Nisancioglu, K. H.: Melting of Northern Greenland during the last interglaciation, The Cryosphere, 6, 1239–1250, doi:10.5194/tc-6-1239-2012, 2012. 1737, 1744, 1745

CAPE-Last Interglacial Project Members: Last Interglacial Arctic warmth confirms polar amplification of climate change, Quaternary Sci. Rev., 25, 1383–1400, 2006. 1736, 1740, 1749

Carlson, A. E., Stoner, J. S., Donnelly, J. P., and Hillaire-Marcel, C.: Response of the southern Greenland ice sheet during the last two deglaciations, Geology, 36, 359–362, doi:10.1130/G24519A.1, 2008. 1750, 1753, 1754

Colville, E. J., Carlson, A. E., Beard, B. L., Hatfield, R. G., Stoner, J. S., Reyes, A. V., and Ullman, D. J.: Sr-Nd-Pb isotope evidence for ice-sheet presence on southern Greenland during the Last Interglacial, Science, 333, 620–623, doi:10.1126/science.1204673, 2011. 1750, 1753, 1754

Cuffey, K. M. and Marshall, S. J.: Substantial contribution to sea-level rise during the last interglacial from the Greenland ice sheet, Nature, 404, 591–594, 2000. 1737, 1744

De Vernal, A. and Hillaire-Marcel, C.: Natural variability of Greenland climate, vegetation and ice volume during the past million years, Science, 320, 1622–1625, doi:10.1126/science.1153929, 2008. 1750, 1753, 1754

Dutton, A. and Lambeck, K.: Ice volume and sea level during the Last Interglacial, Science, 337, 216–219, doi:10.1126/science.1205749, 2012. 1736

EPICA community members: One-to-one coupling of glacial climate variability in Greenland and Antarctica, Nature, 444, 195–198, doi:10.1038/nature05301, 2006. 1740

Ettema, J., Van den Broeke, M. R., Van Meijgaard, E., Van de Berg, W. J., Bamber, J. L., Box, J. E., and Bales, R. C.: Higher surface mass balance of the Greenland ice sheet revealed by high-resolution climate modeling, Geophys. Res. Lett., 36, L12501, doi:10.1029/2009GL038110, 2009. 1738, 1739, 1743

Fettweis, X., Hanna, E., Gallée, H., Huybrechts, P., and Erpicum, M.: Estimation of the Greenland ice sheet surface mass balance for the 20th and 21st centuries, The Cryosphere, 2, 117–129, doi:10.5194/tc-2-117-2008, 2008. 1737

Francis, D. R., Wolfe, A. P., Walker, I. R., and Miller, G. H.: Interglacial and Holocene temperature reconstructions based on midge remains in sediments of two lakes from Baffin Island, Nunavut, Arctic Canada, Palaeogeogr. Palaeocl., 236, 107–124, 2006. 1749

Fyke, J. G., Weaver, A. J., Pollard, D., Eby, M., Carter, L., and Mackintosh, A.: A new coupled ice sheet/climate model: description and sensitivity to model physics under Eemian, Last Glacial Maximum, late Holocene and modern climate conditions, Geosci. Model Dev., 4, 117–136, doi:10.5194/gmd-4-117-2011, 2011. 1737, 1744, 1745

Graversen, R. G., Drijfhout, S., Hazeleger, W., Van de Wal, R., Bintanja, R., and Helsen, M.: Greenland's contribution to global sea-level rise by the end of the 21st century, Clim. Dynamics, 37, 1427–1442, 2011. 1740

Greve, R.: Relation of measured basal temperatures and the spatial distribution of the geothermal heat flux for the Greenland ice sheet, Ann. Glaciol., 42, 424–432, 2005. 1742

Helsen, M. M., van de Wal, R. S. W., van den Broeke, M. R., van de Berg, W. J., and Oerlemans, J.: Coupling of climate models and ice sheet models by surface mass balance gradients: application to the Greenland Ice Sheet, The Cryosphere, 6, 255–272, doi:10.5194/tc-6-255-2012, 2012. 1738, 1739, 1740, 1741, 1742, 1743, 1746

Hutter, K.: Theoretical glaciology: material science of ice and the mechanics of glaciers and ice sheets, Reidel Publ. Co., Dordrecht, 1983. 1740

Huybrechts, P.: Sea-level changes at the LGM from ice-dynamic reconstructions of the Greenland and Antarctic ice sheets during the glacial cycles, Quaternary Sci. Rev., 21, 203–231, 2002. 1737, 1744

Jansen, E., Briffa, K. R., Otto-Bliesner, B., and Raynaud, D.: Palaeoclimate, in: Climate Change 2007: The Physical Science Basis, edited by: Solomon, S., Dahe, Q., Manning, M., Marquis, M., Averyt, K., Tignor, M. M. B., LeRoy Miller Jr., H., and Zhenlin, C., Cambridge University Press, Cambridge, 433–497, 2007. 1736, 1746

Johnsen, S. J., Dahl-Jensen, D., Gundestrup, N., Steffensen, J. P., Clausen, H. B., Miller, H., Masson-Delmotte, V., Sveinbjörndottir, A. E., and White, J.: Oxygen isotope and palaeotemperature records from six Greenland ice-core stations: Camp Century, Dye-3, GRIP, GISP2, Renland and NorthGRIP, J. Quaternary Sci., 16, 299–307, 2001. 1742

Kaspar, F., Kühl, N., Cubasch, U., and Litt, T.: A model-data comparison of European temperatures in the Eemian interglacial, Geophys. Res. Lett., 32, L11703, doi:10.1029/2005GL022456, 2005. 1738, 1739, 1748

Kaspar, F., Spangehl, T., and Cubasch, U.: Northern hemisphere winter storm tracks of the Eemian interglacial and the last glacial inception, Clim. Past, 3, 181–192, doi:10.5194/cp-3-181-2007, 2007. 1739, 1740

Koerner, R. M.: Ice Core Evidence for Extensive Melting of the Greenland Ice Sheet in the Last Interglacial, Science, 244, 964–968, doi:10.1126/science.244.4907.964, 1989. 1737

Koerner, R. M. and Fisher, D. A.: Ice-core evidence for widespread Arctic glacier retreat in the Last Interglacial and the early Holocene, Ann. Glaciol., 35, 19–24, 2002. 1737

Kopp, R. E., Simons, F. J., Mitrovica, J. X., Maloof, A. C., and Oppenheimer, M.: Probabalistic assessment of sea level during the last interglacial stage, Nature, 462, 863–868, doi:10.1038/nature08686, 2009. 1736, 1753, 1754

Le Meur, E. and Huybrechts, P.: A comparison of different ways of dealing with isostasy: examples from modelling the Antarctic ice sheet during the last glacial cycle, Ann. Glaciol., 23, 309–317, 1996. 1741

Limited Greenland ice loss during the Eemian

M. M. Helsen et al.

Lhomme, N., Clarke, G. K. C., and Marshall, S. J.: Tracer transport in the Greenland ice sheet: constraints on ice cores and glacial history, Quaternary Sci. Rev., 24, 173–194, 2005. 1737, 1744

McKay, N. P., Overpeck, J. T., and Otto-Bliesner, B. L.: The role of ocean thermal expansion in Last Interglacial sea level rise, Geophys. Res. Lett., 38, L14605, doi:10.1029/2011GL048280, 2011. 1754

NEEM community members: Eemian interglacial reconstructed from a Greenland folded ice core, Nature, 493, 489–494, doi:10.1038/nature11789, 2013. 1737, 1750, 1751, 1752, 1753, 1754, 1770

NGRIP members: High-resolution record of Northern Hemisphere climate extending into the last interglacial period, Nature, 431, 147–151, 2004. 1737, 1742, 1750, 1751, 1752, 1753, 1754, 1770

Otto-Bliesner, B., Marshall, S. J., Overpeck, J. T., Miller, G. H., Hu, A., and CAPE Last Interglacial Project Members: Simulating Arctic climate warmth and icefield retreat in the last interglaciation, Science, 311, 1751–1753, 2006. 1737, 1738, 1744

Overpeck, J. T., Otto-Bliesner, B., Miller, G. H., Muhs, D. R., Alley, R. B., and Kiehl, J. T.: Paleoclimatic evidence for future ice-sheet instability and rapid sea-level rise, Science, 311, 1747–1750, doi:10.1126/science.1115159, 2006. 1736

Petit, J. R., Jouzel, J., Raynaud, D., Barkov, N. I., Barnola, J.-M., Basile, I., Bender, M., Chappellaz, J., Davis, M., Delaygue, G., Delmotte, M., Kotlyakov, V. M., Legrand, M., Lipenkov, V. Y., Lorius, C., Pépin, L., Ritz, C., Saltzman, E., and Stievenard, M.: Climate and atmospheric history of the past 420,000 years from the Vostok ice core, Antarctica, Nature, 399, 429–436, 1999. 1740, 1742

Pollard, D. and DeConto, R. M.: Modelling West Antarctic ice sheet growth and collapse through the past five million years, Nature, 458, 329–332, doi:10.1038/nature07809, 2009. 1754

Quiquet, A., Ritz, C., Punge, H. J., and Salas y Mélia, D.: Greenland ice sheet contribution to sea level rise during the last interglacial period: a modelling study driven and constrained by ice core data, Clim. Past, 9, 353–366, doi:10.5194/cp-9-353-2013, 2013. 1737, 1745

Radić, V. and Hock, R.: Regionally differentiated contribution of mountain glaciers and ice caps to future sea-level rise, Nat. Geosci., 4, 91–94, doi:10.1038/NGEO1052, 2011. 1754

Reerink, T. J., Kliphuis, M. A., and van de Wal, R. S. W.: Mapping technique of climate fields between GCM's and ice models, Geosci. Model Dev., 3, 13–41, doi:10.5194/gmd-3-13-2010, 2010. 1739

Title Page

Abstract | Introduction

Conclusions | References

Tables | Figures

|◀ | ▶|

◀ | ▶

Back | Close

Full Screen / Esc

Printer-friendly Version

Interactive Discussion

Robinson, A., Calov, R., and Ganopolski, A.: Greenland ice sheet model parameters constrained using simulations of the Eemian Interglacial, Clim. Past, 7, 381–396, doi:10.5194/cp-7-381-2011, 2011. 1737, 1744

Sánchez Goñi, M. F., Bakker, P., Desprat, S., Carlson, A. E., Van Meerbeeck, C. J., Peyroin, O., Naughton, F., Fletcher, W. J., Eynaud, F., Rissignol, L., and Renssen, H.: European climate optimum and enhanced Greenland melt during the Last Interglacial, Geology, 40, 627–630, doi:10.1130/G32908.1, 2012. 1748

Siegenthaler, U., Stocker, T. F., Monnin, E., Lüthi, D., Schwander, J., Stauffer, B., Raynaud, D., Barnola, J.-M., Fischer, H., Masson-Delmotte, V., and Jouzel, J.: Stable carbon cycle-climate relationship during the late Pleistocene, Science, 310, 1313–1317, 2005. 1740

Tarasov, L. and Peltier, W. R.: Greenland glacial history, borehole constraints, and Eemian extent, J. Geophys. Res., 108, 2143, doi:10.1029/2001JB001731, 2003. 1737, 1744

Van de Berg, W. J., Van den Broeke, M., Ettema, J., Van Meijgaard, E., and Kaspar, F.: Significant contribition of insolation to Eemian melting of the Greenland ice sheet, Nat. Geosci., 4, 679–683, doi:10.1038/ngeo1245, 2011. 1738, 1739, 1745, 1748, 1764

Van de Wal, R. S. W.: The importance of thermodynamics for modeling the volume of the Greenland ice sheet, J. Geophys. Res., 104, 3889–3898, 1999. 1738, 1740

Weertman, J.: The theory of glacial sliding, J. Glaciol., 5, 287–303, 1964. 1741

Willerslev, E., Cappellini, E., Boomsma, W., Nielsen, R., Hebsgaard, M. B., Brand, T. B., Hofreiter, M., Bunce, M., Poinar, H. N., Dahl-Jensen, D., Johnsen, S., Steffensen, J. P., Bennike, O., Schwenninger, J.-L., Nathan, R., Armitage, S., de Hoog, C., Alfimov, V., Christl, M., Beer, J., Muscheler, R., Barker, J., Sharp, M., Penkman, K. E. H., Haile, J., Taberlet, P., Gilbert, M. T. P., Casoli, A., Campani, E., and Collins, M.: Ancient biomolecules from deep ice cores reveal a forested southern Greenland, Science, 317, 111–114, 2007. 1737, 1751, 1753, 1754

Winograd, I. J., Landwehr, J. M., Ludwig, K. R., Coplen, T. B., and Riggs, A. C.: Duriation and structure of the past four interglaciations, Quatern. Res., 48, 141–154, 1997. 1740

Title Page

Abstract | Introduction

Conclusions | References

Tables | Figures

|◄ | ►|

◄ | ►

Back | Close

Full Screen / Esc

Printer-friendly Version

Interactive Discussion

Table 1. Ice sheet model parameter values.

Parameter	Symbol	Value	Unit
gravitational acceleration	g	9.81	$\mathrm{m\,s^{-2}}$
ice density	ρ_i	910	$\mathrm{kg\,m^{-3}}$
sea water density	ρ_s	1028	$\mathrm{kg\,m^{-3}}$
Glen's flow law exponent	n	3	–
flow enhancement	m	3	–
sliding coefficient	A_s	1.8×10^{-10}	$\mathrm{m^8\,N^{-3}\,yr^{-1}}$
geothermal heat flux	G	54.5	$\mathrm{mW\,m^{-2}}$
lithosph. flex. rigidity	D	1×10^{25}	$\mathrm{N\,m}$
astenosphere density	ρ_a	3300	$\mathrm{kg\,m^{-3}}$
bedrock relaxation time	τ	3000	yr
atmospheric lapse rate	γ_{atm}	−7.4	$\mathrm{K\,km^{-1}}$

Table 2. Summary of sensitivity experiments.

Experiment	Minimum GrIS volume ($10^{15}\,\text{m}^3$)	SLR (m)	ΔSLR (m)
control	2.35	2.1	0
late start	2.46	1.8	−0.3
early start	2.24	2.4	+0.3
sliding halved	2.51	1.7	−0.4
sliding doubled	2.12	2.7	+0.6
marine melt $100\,\text{m yr}^{-1}$	2.33	2.1	0
marine melt $1000\,\text{m yr}^{-1}$	2.22	2.4	+0.3
SMB $+\,76\,\text{Gt yr}^{-1}$	2.65	1.3	−0.8
SMB $-\,76\,\text{Gt yr}^{-1}$	1.88	3.3	+1.2

Global Climate Model ⟶ Regional Climate Model ⟶ Ice Sheet Model

ECHO-G
(Kaspar et al., 2005)

RACMO2/GR
(Van de Berg et al., 2011)

ANICE
(Helsen et al., 2012)
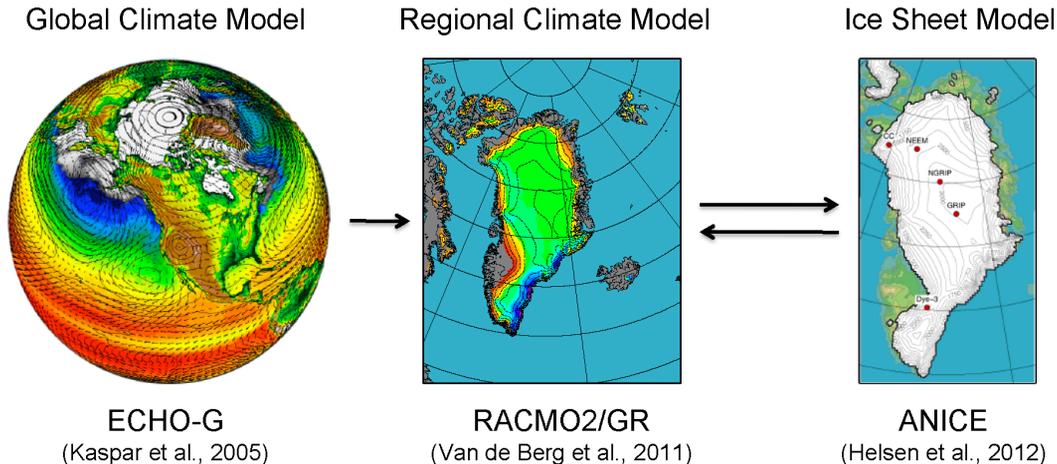
Fig. 1. Schematic outline of the asynchronous model coupling: an Eemian run of the ECHO-G global climate model is used as lateral boundaries for the regional atmospheric climate model, which in turn computes SMB, T_s and refreezing that are used as forcing for the ice sheet model. Every 1.5 kyr, the changed ice sheet topography and extent are updated in the regional atmospheric climate model, after which new fields of SMB, T_s and refreezing are calculated, etc.

Title Page

Abstract | Introduction

Conclusions | References

Tables | Figures

|◀ | ▶|

◀ | ▶

Back | Close

Full Screen / Esc

Printer-friendly Version

Interactive Discussion
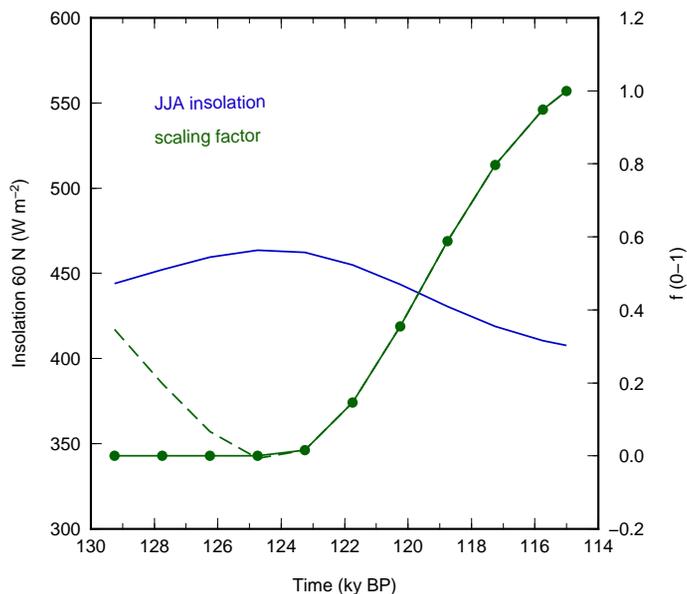
Fig. 2. The scaling factor (green) used to adjust the ECHO-G Eemian fields at the RACMO2 lateral boundaries towards glacial inception values are set proportional to the JJA insolation at 60° N (blue). Dashed green line indicates values of the scaling factor if it would also have been coupled to insolation in the period before 125 kyr BP.
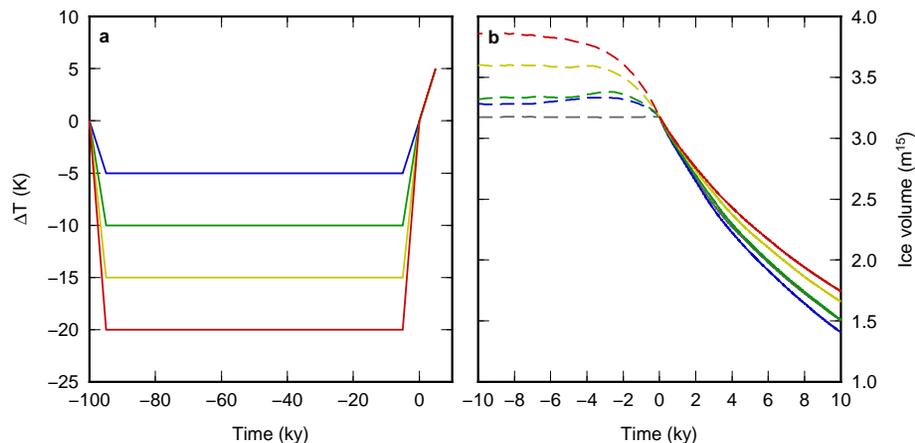
Fig. 3. The dependence of ice sheet sensitivity to their temperature history: **(a)** schematic temperature forcings and **(b)** resulting ice sheet volume evolution. Dashed lines in **(b)** are the ice sheet volume response of the different forcings from **(a)**. Each of these simulation is continued until the ice volume of the steady-state ice sheet (grey dashed line) is reached. Results in **(b)** are horizontally shifted such that they have identical ice volume at $t = 0$. After $t = 0$, all simulations are forced with the same Eemian climatology from Van de Berg et al. (2011) for 10 kyr.
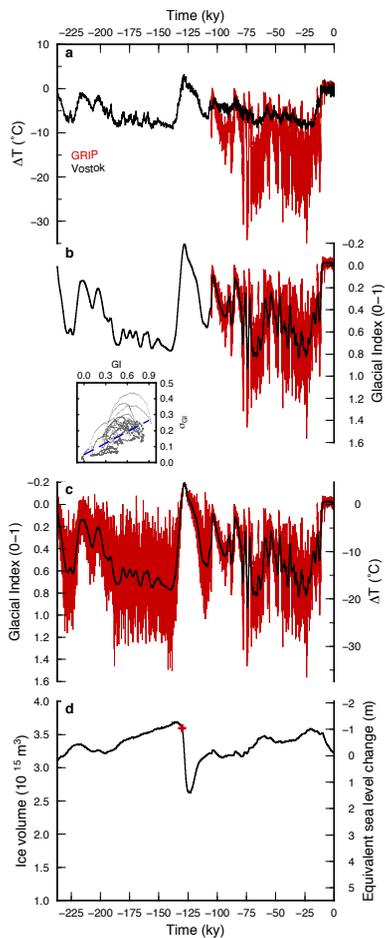
Fig. 4. Caption on next page.

Fig. 4. Climate forcing used to initialise the ice sheet. **(a)** Near-surface air temperature proxies for the GRIP and Vostok ice cores; **(b)** glacial indices derived from these ice core records, with 20 yr resolution (red) and after applying a Gaussian filter (black). Inset in **(b)** is a scatter plot of the standard deviation in the glacial index (GI) within a 3 kyr bandwidth filter as a function of the mean GI. **(c)** Added high frequency variability of GI in the pre 105 kyr BP period. Right axis shows corresponding climate record. **(d)** Resulting simulated ice volume using the climate forcing from **(c)**.
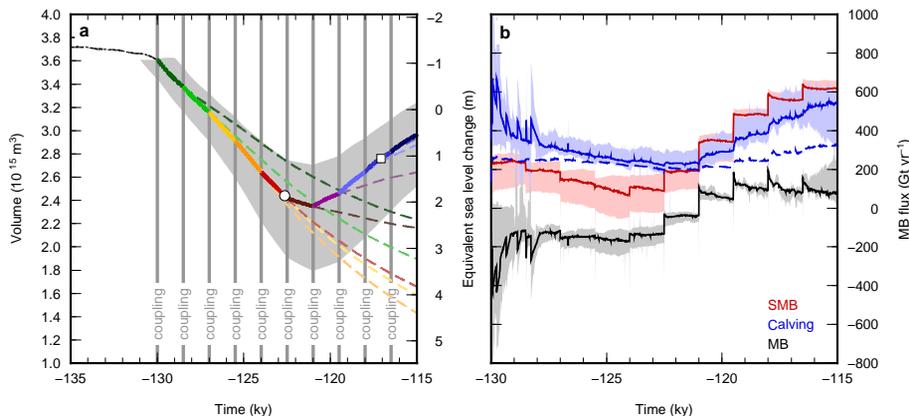
Fig. 5. Eemian ice volume changes and mass balance components. **(a)** Simulated GrIS volume change and equivalent sea level contribution. The colours indicate different climate forcings. Dashed lines show ice volume evolution without additional coupling. Circle (square) indicate the timing of ice margin retreat (readvance) at Dye-3. **(b)** Time series of SMB (red), ice discharge (calving, blue) and MB (black). The blue dashed line represents the calving flux along the southeastern margin, south of 68° N (see text). Background shading represents the uncertainty estimate.
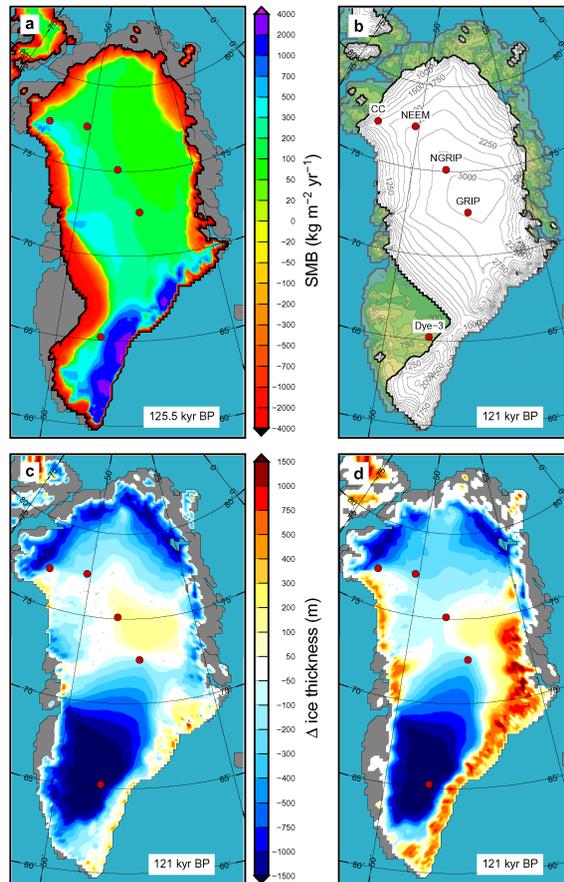
Fig. 6. SMB, minimum extent and ice thickness anomaly. **(a)** SMB pattern during Eemian optimum conditions; **(b)** simulated minimum GrIS at 121 kyr BP; **(c)** difference in ice thickness compared to present-day simulation; **(d)** difference in ice thickness compared to present-day measurements. An animation of GrIS evolution from 130–115 kyr BP is available online.
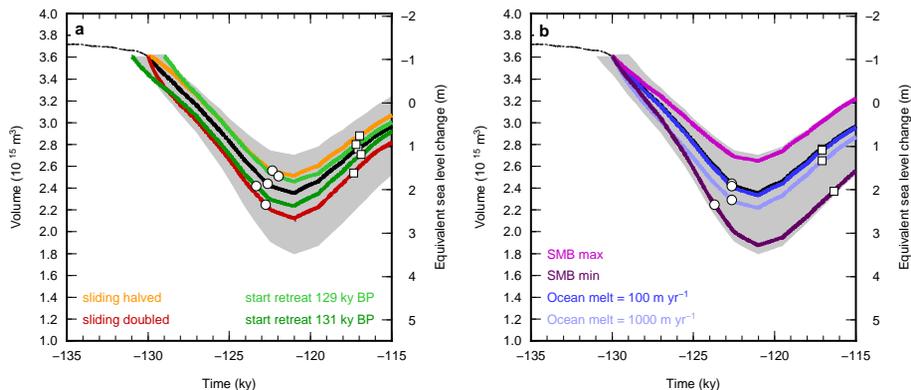
Fig. 7. Simulated GrIS volume change and equivalent sea level contribution through the Eemian in different sensitivity experiments: **(a)** experiments using a different start of the Eemian warming and a perturbed sliding velocity, **(b)** experiments with additional mass loss due to ice–ocean contact and perturbations in the SMB forcing. Circles (squares) indicate the timing ice margin retreat (readvance) at Dye-3. Complete retreat from the Dye-3 location did not occur in the SMBmin experiment, when the ice margin remained exactly on that location during the minimum extent.
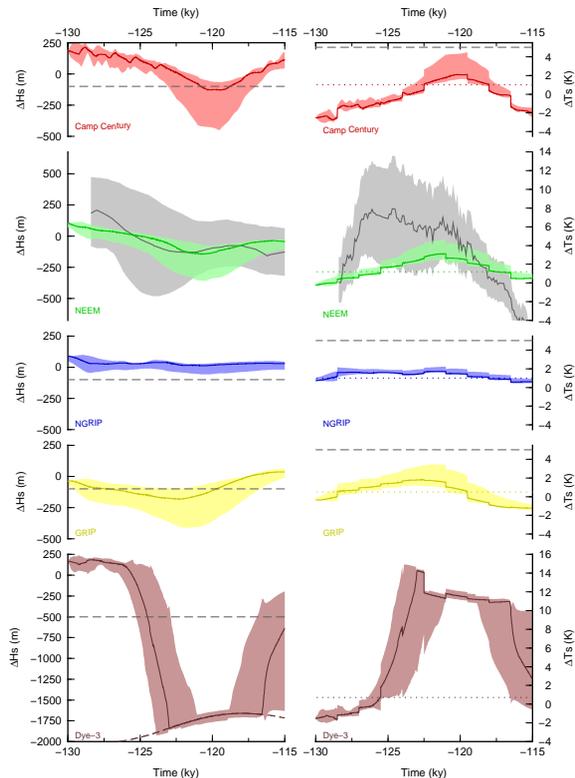
Fig. 8. Surface elevation and temperature at deep drilling sites. Time series of surface height change (left panels) and mean annual surface temperature (right panels) at five deep drilling locations, relative to present-day. Estimates of minimum elevation and maximum air temperature as reconstructed from ice cores (NGRIP members, 2004) are shown as dashed grey lines, solid grey lines represent results from the NEEM ice core record (NEEM community members, 2013), and the lower (brown) dashed line in bottom panel denotes bedrock. Note that due to their close proximity, we do not make a distinction between GRIP and GISP2 in our results.

Title Page

Abstract | Introduction

Conclusions | References

Tables | Figures

|◄ | ►|

◄ | ►

Back | Close

Full Screen / Esc

Printer-friendly Version

Interactive Discussion